Preclinical fluorescent mouse models of pancreatic cancer

Michael Bouvet*[a] and Robert M. Hoffman [a,b]
[a]University of California San Diego, 3855 Health Sciences Drive, La Jolla, CA 92093-0987
[b]AntiCancer, Inc., 7917 Ostrow Street, San Diego, CA 92111

ABSTRACT

Here we describe our cumulative experience with the development and preclinical application of several highly fluorescent, clinically-relevant, metastatic orthotopic mouse models of pancreatic cancer. These models utilize the human pancreatic cancer cell lines which have been genetically engineered to selectively express high levels of the bioluminescent green fluorescent (GFP) or red fluorescent protein (RFP). Fluorescent tumors are established subcutaneously in nude mice, and tumor fragments are then surgically transplanted onto the pancreas. Locoregional tumor growth and distant metastasis of these orthotopic implants occurs spontaneously and rapidly throughout the abdomen in a manner consistent with clinical human disease. Highly specific, high-resolution, real-time visualization of tumor growth and metastasis may be achieved *in vivo* without the need for contrast agents, invasive techniques, or expensive imaging equipment. We have shown a high correlation between florescent optical imaging and magnetic resonance imaging in these models. Alternatively, transplantation of RFP-expressing tumor fragments onto the pancreas of GFP-expressing transgenic mice may be used to facilitate visualization of tumor-host interaction between the pancreatic tumor fragments and host-derived stroma and vasculature. Such *in vivo* models have enabled us to serially visualize and acquire images of the progression of pancreatic cancer in the live animal, and to demonstrate the real-time antitumor and antimetastatic effects of several novel therapeutic strategies on pancreatic malignancy. These fluorescent models are therefore powerful and reliable tools with which to investigate human pancreatic cancer and therapeutic strategies directed against it.

Keywords: GFP, RFP, pancreas, pancreatic cancer, mouse models

1. INTRODUCTION

Pancreatic cancer is often a fatal disease with 5-year survival rates of only 1-4% (1, 2). It is the fourth leading cause of cancer related mortality in the United States. Reasons for low survival in this disease include aggressive tumor biology, high metastatic potential, and late presentation at the time of diagnosis (3, 4). The symptoms of pancreatic cancer may include jaundice, pain, weight loss, digestive problems, and new onset diabetes (5). By the time an individual with pancreatic cancer develops these symptoms, the tumor has often reached a large size and metastasized to other organs including liver, lung, and peritoneum (4). Although chemotherapy can offer some palliation, it is not curative and the median survival is less than 6 months. For the few patients who have localized disease, surgical resection offers the only chance for cure. However, even with potentially curative surgery the five-year survival rates are only 15-20% (1). Clearly, techniques for earlier diagnosis and new treatment modalities need to be explored if progress is to be made. In an effort to help develop more effective treatment modalities for pancreatic cancer and improve detection, we and others have developed orthotopic models of human pancreatic cancer in the nude mouse that simulate tumor growth, progression, and metastasis and allow for testing of novel treatment strategies (6-15).

Mouse models based on athymic mice have been used for human cancer for the past several decades. However, metastatic rates from subcutaneous or intramuscular xenografts have been low or non-existent, even from tumors that were highly metastatic in the patient from whom the tissues were derived (16, 17). Work from a number of laboratories indicates that implanting human tumor cells orthotopically in the corresponding organ of nude mice results in much higher metastatic rates. For instance, dissociated human colon cancer cells, when grown in culture and subsequently injected into the cecum of nude mice, produce tumors that eventually metastasize to the liver, showing that orthotopic implantation can enhance the metastatic capability of human tumor cells in nude mice (18). Similar results have been achieved for orthotopic implantation of cell lines of human lung cancer, bladder cancer, melanoma, breast cancer, stomach, colon, and head and neck cancer.

In the 1980s, investigators first reported metastatic models of human pancreatic cancer using orthotopic implantation of tumor-cell suspensions, which resulted in invasive tumor growth and subsequent metastases (8, 19).

Genetically Engineered and Optical Probes for Biomedical Applications IV, Samuel Achilefu, Darryl J. Bornhop, Ramesh Raghavachari, Alexander P. Savitsky, Rebekka M. Wachter, Eds., Proc. of SPIE Vol. 6449, 64490X, (2007) · 1605-7422/07/$18 · doi: 10.1117/12.708060

Vezeridis et al used pancreatic tumor tissue for orthotopic transplantation, resulting in extensive local growth, and metastases to liver, lung, and lymph nodes (10). In 1992, we used histologically intact patient specimens of pancreatic cancer for orthotopic transplantation to nude mice to construct a metastatic model of human pancreatic cancer (11). This model resembled the clinical picture of pancreatic cancer including: 1) extensive local tumor growth, 2) extension of the locally growing human pancreatic cancer to the nude mouse stomach and duodenum, 3) metastases of the human pancreatic tumor to the nude-mouse liver and regional lymph nodes, and 4) distant metastases of the human pancreatic tumor to the nude-mouse adrenal gland, diaphragm, and mediastinal lymph nodes (11).

The following year, we described use of this patient-like model of human pancreatic cancer for the in-vitro and in-vivo evaluation of the antitumor activity of 5-fluoroocuracil (5-FU) and mitomycin-C (MMC) (13). The antitumor activity of these agents was initially determined in an in-vitro histoculture drug-response assay and inhibition rates were 5.6% for 5-FU and 39.4% for MMC. When the antitumor activities of 5-FU against PANC-4 was determined in vivo using the nude mouse orthotopic transplant treatment model, slight local tumor growth inhibition with equivalent incidence of metastases to the liver and the peritoneum as the control were observed in the mice treated with 5-FU. In contrast, mice treated with MMC had considerably reduced local tumor growth without liver and peritoneal metastases. Thus the histoculture drug response assay in combination with the orthotopic transplant metastatic model provided for the first time a paradigm for evaluation of agents that may be effective against not only locally growing human pancreatic cancer but resulting metastases as well.

A number of approaches have been taken to label tumor cells to visualize and track them in vivo. Previous attempts to genetically label tumor cells for tracking purposes used the *Escherichia coli* β-galactosidase (*lacZ*) gene to detect micrometastases (20). However, detection of *lacZ* requires extensive histological preparation, with sacrifice of the tissue and/or animal: therefore, it was not possible to image, visualize, and study tumor cells in real-time in viable fresh tissue or in the live animal.

The ability to confer real-time visualization and imaging of tumor growth and progression in viable fresh tissue and in the live animal would be an important factor in the development of a real-time reporter gene for metastasis and recurrence. Several approaches have been developed with this goal in mind: Fukumura et al and Chambers et al labeled tumor tissue with fluorescent dyes. However, these methods are not suitable for long-term metastasis studies (21, 22). Weissleder et al have infused tumor-bearing animals with protease-activated near-infrared fluorescent probes (23). Tumors with appropriate proteases could activate the probes and could be imaged externally. The limits to such a system include much higher liver to tumor background precluding liver metastasis imaging, which is among the most important metastatic sites; the stated time limit of 96 hours, which precludes growth and efficacy studies; the requirement of appropriate tumor protease activity; and the requirement of selective tumor delivery of the probes.

Another attempt involved insertion of the luciferase gene into tumor cells such that they emit light (24). However, luciferase enzymes transferred to mammalian cells require the exogenous injected delivery of their luciferin substrate, an invasive and impractical requirement in an intact animal. The resolution of this approach is low, due to low signal strength, requiring anesthesia since long periods are needed for photon counting. With this technology, there is insufficient photon flux to form a true image. Also, it is not known whether luciferase genes can function stably over significant time periods in tumors and in the metastases derived from them.

It became clear that higher signal strength, specificity, resolution, and physiological conditions were necessary to report the natural course of tumor progression and metastasis on a real-time basis. The green fluorescent protein (GFP) gene, cloned from the bioluminescent jellyfish *Aequorea victoria,* was chosen to satisfy these conditions because it has demonstrated its great potential for use as a cellular marker (25-27). GFP cDNA encodes a 283-aa monomeric polypeptide with a molecular mass of 27 kDa that requires no other *Aequorea* proteins, substrates, or cofactor to fluoresce (28, 29). GFP gene gain-of-function bright mutants have been generated by various techniques that have been humanized for high expression (30-33).

A major advantage of GFP-expressing tumor cells is that imaging requires no preparative procedures, contrast agents, substrates, anesthesia, or light-tight boxes as do other imaging techniques (34). GFP imaging is thus uniquely suited for whole-body imaging of tumor growth and metastases in live animals (35-37). We have developed technology that has enabled the stable transduction of the GFP gene into a large series of human tumor cell lines (38-49). The tumor cell lines were able to stably express GFP at high levels both in vitro and in vivo. We have previously demonstrated the important parameter that GFP-expressing cancer cells could be directly visualized in fresh tissues of transplanted animals at a very high resolution down to the single cell level (38-42). With this technology, we were able to visualize tumor cells that had seeded with or without subsequent colonization in all the major organs, including liver, lung, brain, spinal cord, axial skeleton, and lymph nodes (38-42). We have developed orthotopic GFP metastatic models of lung cancer (43), prostate cancer (44), melanoma (45), and colon cancer (46). These results demonstrated that GFP gene-transfected

tumor cells represent a new tool to study tumor cell growth, dissemination, invasion, metastasis, and progression through all stages.

Recently, we described an in vivo model of GFP-expressing pancreatic cancer in the nude mouse (6, 7). To understand the metastatic pattern of pancreatic cancer, we developed stable high-expression GFP transductants of human pancreatic cancer cell lines. Fragments of subcutaneous-growing tumors were implanted by surgical orthotopic implantation (SOI) in the pancreas of nude mice or by portal vein injection of a cell suspension. Subsequent micrometastases were visualized by GFP fluorescence in the peritoneum, periportal lymph nodes, liver, and lung as well as other sites in the abdominal cavity. The use of GFP-expressing MiaPaCa-2 and BxPC-3 cells transplanted by SOI or by portal vein injection revealed the extensive metastatic potential of pancreatic cancer. Furthermore, the primary tumor and subsequent metastasis were visualized by whole body imaging through the skin of the nude mouse without the need for laparotomy (7). Such visualization can be a practical and convenient way to follow metastasis in a "real-time" fashion. We have also described a novel, highly metastatic model of pancreatic cancer that utilizes pancreatic cancer cells engineered to express very high levels of *Discosoma sp.* red fluorescent protein (RFP) (50-56). These RFP-expressing pancreatic tumors can be implanted into the pancreas of transgenic GFP nude mice to create dual color models to study tumor host interactions (57, 58). These new metastatic models can play a critical role in the study of the mechanism of metastasis in pancreatic cancer and in screening of therapeutics that prevent or reverse this process.

2. GREEN FLUORESCENT PROTEIN (GFP) MODELS OF PANCREATIC CANCER

2.1 GFP Models of pancreatic cancer

Several years ago, we described an in vivo model of GFP-expressing pancreatic cancer in the nude mouse (6, 7). To understand the metastatic pattern of pancreatic cancer, we developed stable high-expression GFP transductants of human pancreatic cancer cell lines. Fragments of subcutaneous-growing tumors were implanted by surgical orthotopic implantation (SOI) in the pancreas of nude mice or by portal vein injection of a cell suspension. Subsequent micrometastases were visualized by GFP fluorescence in the peritoneum, periportal lymph nodes, liver, and lung as well as other sites in the abdominal cavity (Figure 1). The use of GFP-expressing MiaPaCa-2 and BxPC-3 cells transplanted by SOI or by portal vein injection revealed the extensive metastatic potential of pancreatic cancer at the cellular level in vivo. Furthermore, the

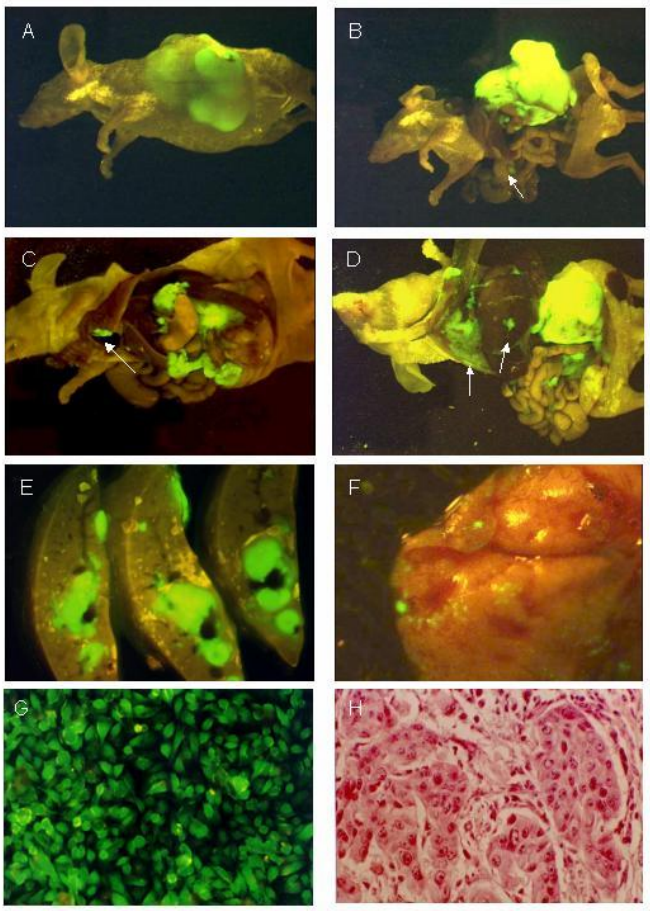

Figure 1 A) The BxPC-3-GFP pancreatic tumor transplanted by surgical orthotopic implantation (SOI) is externally visualized with fluorescence through the skin of the nude mouse. B) Laparotomy of the same mouse in (A) showing locally advanced BxPC-3-GFP tumor with portal lymph node metastases. C) The primary tumor formed in the pancreas at 12 weeks after SOI is visualized under bright-field microscopy. Numerous metastases and micrometastases can be visualized by GFP under fluorescence microscopy to the stomach, spleen, periportal nodes (arrow), liver, and mediastinum (arrow). D) MIA PaCa-2-GFP tumor at week-10 post-SOI. Left arrow shows diaphragm metastases and right arrow shows liver metastases. E) Multiple high expressing GFP liver metastases are noted under fluorescence microscopy. F) GFP-expressing lung metastases are noted. G) The human pancreatic cancer cell line MIA PaCa-2 was transduced with the RetroXpress vector pLEIN that expresses enhanced GFP and the neomycin resistance gene on the same bicistronic message. The stable high expression clone was selected in 800 μg/ml of G418. H) H&E section of MIA PaCa-2-GFP tumor.

primary tumor and subsequent metastasis were visualized by whole body imaging through the skin of the nude mouse without the need for laparotomy (7). Such visualization can be a practical and convenient way to follow metastasis in a "real-time" fashion. These new metastatic models can play a critical role in the study of the mechanism of metastasis in pancreatic cancer and in screening of therapeutics that prevent or reverse this process.

2.2 Tumor selective metastatic organ targeting (6)

Figure 2 represents the incidence of metastasis in each model at week-20 post-SOI. The BxPC-3-GFP cell line produced locally-advanced, invasive tumors that metastasized regionally selectively to the spleen and the retroperitoneum with distant liver metastases very rare (Figure 2A). In contrast, metastases in the MIA-PaCa-2 model were selective to distant sites in the portal lymph nodes and liver with regional retroperitoneal lymph node metastasis very rare (Figure 2B).

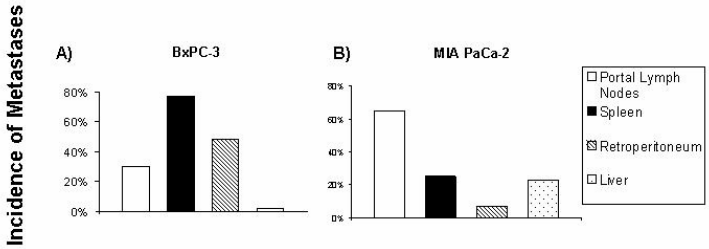

Figure 2. Site-specific metastases in orthotopic models of human pancreatic cancer. A) BxPC-3-GFP B) MIA-PaCa-2-GFP. Forty-four and 26 mice were used for the BxPC-3-GFP and MIA-PaCa-2 models, respectively. The y-axis represents cumulative percentage of mice with metastasis.

2.3 Real-time simultaneous whole-body imaging of BxPC-3-GFP tumor and multiple metastatic growth (7)

Consecutive whole-body simultaneous images of the primary BxPC-3-GFP pancreatic tumor, spleen, bowel, and omentum metastases are shown in Figure 3A. These images were simultaneously obtained in a single animal on day-46, day-50, day-57, and day-64 after SOI. In each of the sites, tumor growth and progression were quantified with image analysis. Growth curves (Figure 3B) for the primary tumor and metastases at each of the above sites were constructed from the whole-body images. Thus, simultaneous metastases development can be quantitated with whole-body imaging.

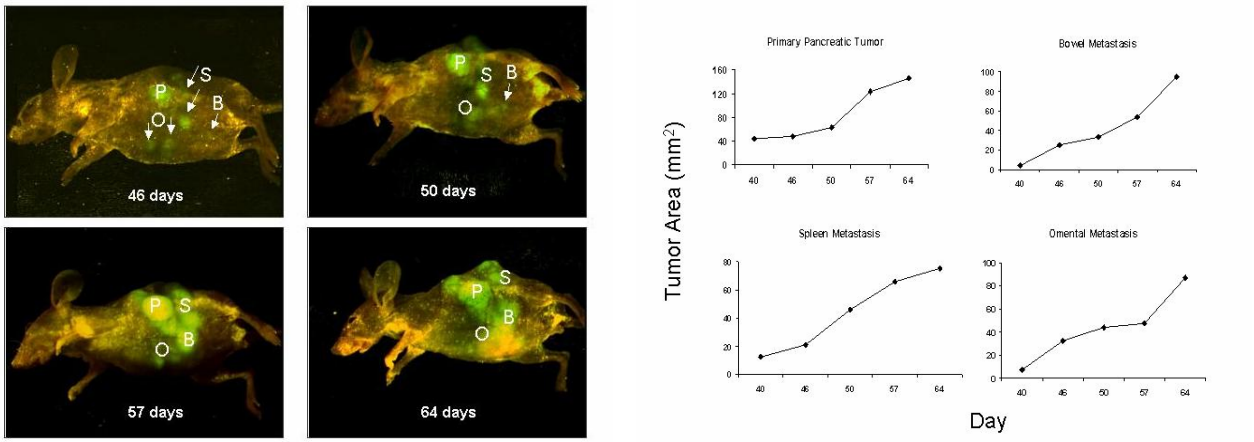

Figure 3. Consecutive external whole-body images of internally-growing BxPC-3-GFP tumors. A series of external fluorescence images of the BxPC-3-GFP pancreatic tumor in a single animal was obtained from day-46 to day-64 after SOI of BxPC-3-GFP in a nude mouse. On right: growth curves for primary pancreatic tumor (P), splenic metastasis (S), omental metastases (0), and bowel metastasis (B) as determined by whole-body imaging.

2.4 Sequential intravital images of omental and liver micrometastasis of BxPC-3-GFP (7)

A series of internal intravital fluorescence images of an omental micrometastasis from a BxPC-3-GFP pancreatic tumor in a single animal was obtained from day-36 to day-70 after SOI of BxPC-3-GFP in a nude mouse. The images were acquired during a laparotomy procedure. As determined by intravital imaging, the size of the metastatic lesion grew progressively with time (Figure 4). Figure 5 shows a series of intravital fluorescence images of liver micrometastases following SOI of BxPC-3-GFP in nude mice.

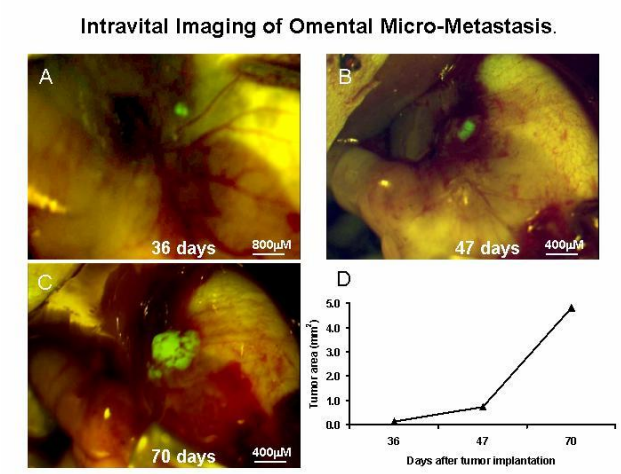

Figure 4. Sequential intravital images of omental micrometastasis of BxPC-3-GFP. A series of internal fluorescence images of an omental micrometastasis from a BxPC-3-GFP pancreatic tumor in a single animal was obtained from day-36 to day-70 after SOI of BxPC-3-GFP in a nude mouse during a laparotomy procedure (Panels A-C). As determined by internal imaging, the size of the metastatic lesion grew progressively with time (Panel D).

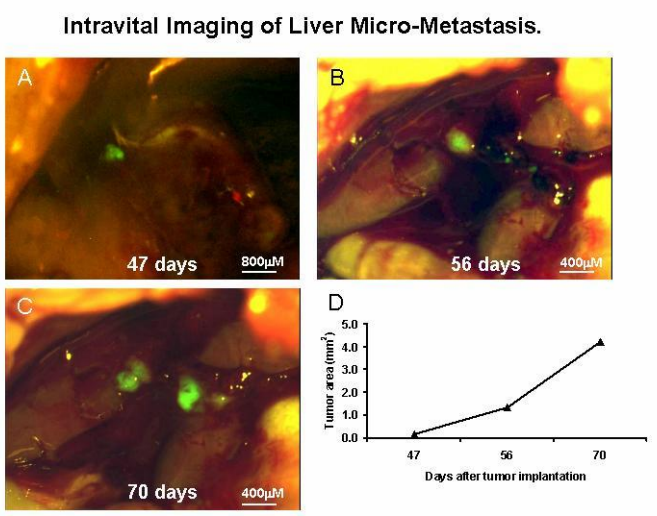

Figure 5. Sequential intravital images of liver micrometastasis of BxPC-3-GFP. Internal images of liver metastases following SOI of BxPC-3-GFP tumor in nude mice were obtained during a laparotomy procedure (Panels A-C). As determined by internal imaging, the area of the metastatic lesions increased over time.

3. RED FLUORESCENT PROTEIN (RFP) MODELS OF PANCREATIC CANCER

3.1 Red Fluorescent Protein Models of pancreatic cancer (50-56)

We described a novel, highly metastatic model of pancreatic cancer that utilizes pancreatic cancer cells engineered to express very high levels of *Discosoma sp.* red fluorescent protein (RFP). This model clinically resembles human pancreatic cancer in its pattern of growth and metastasis. It rapidly and reliably produces distant metastatic disease, and frequently gives rise to malignant abdominal ascites and peritoneal carcinomatosis. Moreover, the enhanced fluorescence of this

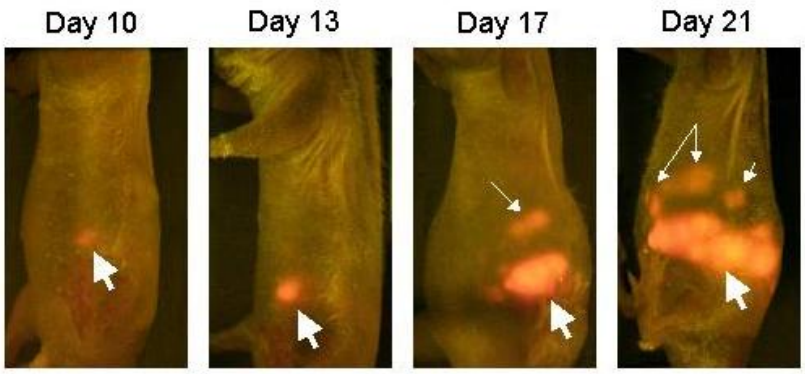

Figure 6. RFP tumor fluorescence enabled real-time, whole-body imaging of tumor growth and metastasis of MIA-PaCa-2-RFP tumors after surgical orthotopic implantation. Panels represent sequential fluorescent imaging of a single mouse taken on days 10, 13, 17 and 21 after SOI. Progressive primary tumor growth and the development of metastases are clearly visualized through the skin in the live animal. Heavy arrow = primary tumor, thin arrows = metastatic tumor.

model enables real-time visualization and imaging of pancreatic tumor growth and metastasis in the live animal, and permits identification of both macro- and micrometastases. These features make the model an ideal system with which to study the effects of novel antineoplastic agents on tumor growth and metastasis (Figure 6).

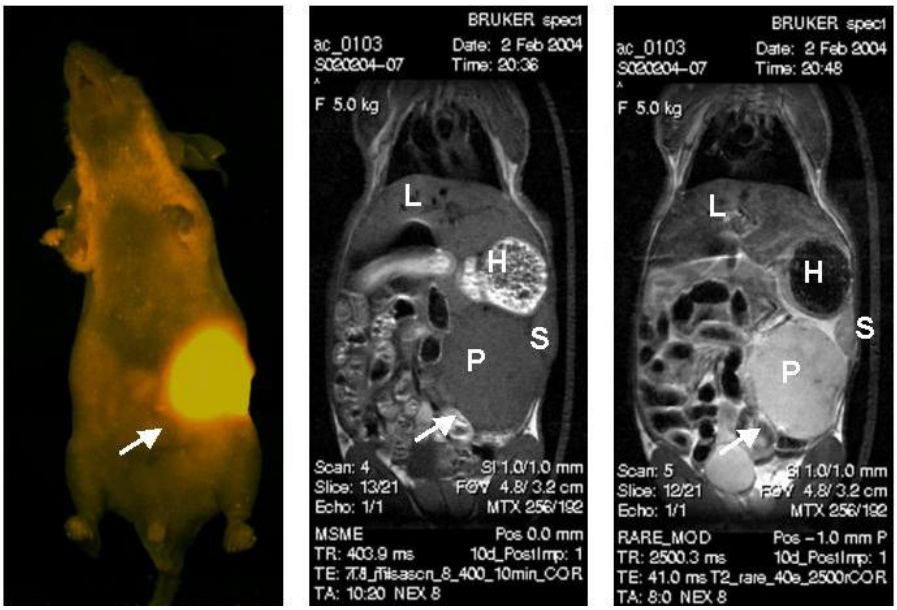

Figure 7: Visualization of early and locally advanced pancreatic malignancy in an orthotopic nude mouse model by fluorescence optical imaging (FOI) and T1- and T2-weighted MRI. Panels represent a single mouse that underwent serial imaging on day 10 after surgical orthotopic implantation of fluorescent MIA-PaCa-2-RFP human pancreatic cancer fragments. Primary tumor was clearly visible using each imaging strategy. P = pancreas, L= liver, H = stomach, S = spleen.

imaged depends on their size. It should be noted that this sensitivity was achieved with a simple light box equipped with a 50-watt mercury lamp. Laser light sources now available to us enable greater sensitivity and resolution even deeper in the animal (Bouvet and Hoffman, unpublished data). Our recent studies (54) compared RFP-expressing pancreatic tumors to MRI (see Figure 7). The fluorescent tumor size can be quantified using image quantification software as we have previously described (52, 56) and appears to be at least as sensitive as MRI.

In our recently described RFP model of pancreatic cancer, we have performed correlation studies to validate external imaging (50, 52, 55). To confirm a correlation between tumor burden, as determined by externally visualized RFP fluorescence, and standard measurements of tumor volume, the primary tumor of each mouse was used. Primary tumor volume was first calculated using the formula (long diameter x short diameter^2)/2, where long diameter and short diameter measurements were precisely obtained in

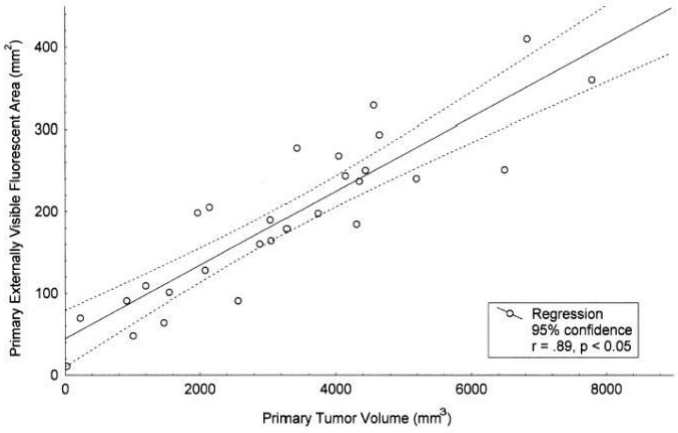

Figure 8. Red fluorescent area quantified using external fluorescence imaging correlated strongly with tumor volume measured directly. At autopsy, measurement of externally visualized fluorescent area and direct measurements of the primary tumor of each mouse were obtained. A significant correlation ($r = 0.89$, $P < 0.05$) was observed between these values.

3.2 Sensitivity of fluorescent imaging

We have previously published data that describes in detail the reproducibility and sensitivity of our non-invasive fluorescence imaging systems demonstrating that single cells can be imaged. Using fairly simple equipment including a CCD camera and light box, we have reproducibly and non-invasively quantitated tumor growth and response to therapy (6, 7, 38, 46, 49-52, 55, 56, 59-61). With regard to the sensitivity of fluorescent imaging, we have shown that when human pancreatic cancer was surgically orthotopically implanted into nude mice, whole-body optical images showed, in real time, growth of the primary tumor and its metastatic lesions in the liver and other organs (6, 7, 44). The depth to which metastasis (46) and micrometastasis could be

the open animal. The externally-visualized RFP fluorescent area was then determined as previously described by placing the mouse in a fluorescent light box equipped with a fiberoptic light source of 470 nm. At each imaging time point, real-time determination of tumor burden was performed by quantifying fluorescent surface area, as described previously (7, 50). The correlation coefficient ($r = 0.89$) between tumor volume and RFP fluorescence was highly significant ($p < 0.05$) (see Figure 8).

We can increase the sensitivity of our system down to the single cell level by the use of a simple skin flap in the mouse as we have previously published (49). Strong fluorescence labeling with green and red fluorescent protein along with inexpensive video detectors, positioned externally to the mouse, allows the monitoring of details of tumor growth, angiogenesis, and metastatic spread. Opening a reversible skin-flap in the light path markedly reduces signal attenuation, increasing detection sensitivity many-fold. The observable depth of tissue is thereby greatly increased and many tumors that were previously hidden are now clearly observable. In our previous publication (49), single tumor cells, expressing GFP, were seeded on the brain and imaged through a scalp skin-flap. Lung tumor micro foci representing a few cells were viewed through a skin-flap over the chest wall, while contralateral micrometastases were imaged through the corresponding skin-flap. Pancreatic tumors and their angiogenic microvessels were imaged by means of a peritoneal wall skin-flap.

4. DUAL COLOR MODELS OF PANCREATIC CANCER

4.1 Dual-color imaging of nascent blood vessels vascularizing pancreatic cancer in an orthotopic model demonstrates antiangiogenesis efficacy of gemcitabine (57)

The stem cell marker nestin recently has been shown to be expressed in nascent blood vessels in nestin-driven green fluorescent protein (ND-GFP) transgenic nude mice. We visualized by dual-color fluorescence imaging tumor angiogenesis in the ND-GFP transgenic nude mice after orthotopic transplantation of the MIA PaCa-2 human pancreatic cancer line expressing RFP. Mice were treated with gemcitabine at 150 mg/kg/dose on days 3, 6, 10, and 13 after tumor implantation. At day 14, mice were sacrificed and mean nascent blood vessel density and tumor volume were calculated and compared to control mice. Nestin was highly expressed in proliferating endothelial cells and nascent blood vessels in the growing tumor (Figures 9 and 10). Results of immunohistochemical staining showed that CD31 co-localized in ND-GFP-expressing nascent blood vessels. The density of nascent blood vessels in the tumor was readily quantitated. Gemcitabine significantly decreased the mean nascent blood vessel density in the tumor as well as decreased tumor volume. The dual-color model of the ND-GFP nude mouse orthotopically implanted with RFP-expressing pancreatic tumor cells enabled the simultaneous visualization and quantitation of tumor angiogenesis and tumor volume. These results demonstrated for the first time that gemcitabine is an inhibitor of angiogenesis as well as tumor growth in pancreatic cancer. The results have important implications for the clinical application of gemcitabine in this disease.

4.2 Dual-color imaging of nascent blood vessels vascularizing pancreatic cancer in an orthotopic model demonstrates antiangiogenesis efficacy of gemcitabine (58)

Nascent angiogenesis of pancreatic cancer liver metastasis in the ND-GFP transgenic nude mice after splenic injection of low-passage xPA-1 human pancreatic cancer cells expressing RFP was visualized by dual-color fluorescence imaging. ND-GFP was highly expressed in proliferating endothelial cells and nascent blood vessels in the growing liver metastasis. Immunohistochemical staining showed that CD31 co-localized in ND-GFP-expressing nascent blood vessels. The density of nascent blood vessels in the tumor was readily quantitated. Gemcitabine significantly decreased the mean nascent blood vessel density in the pancreatic liver metastases. In conclusion, the dual-color model of the ND-GFP nude mouse with RFP-expressing pancreatic cancer liver metastases, enabled the simultaneous visualization and quantitation of nascent angiogenesis and its response to angiogenesis inhibitors. This model will be useful for understanding the mechanism of angiogenesis of pancreatic cancer liver metastasis and for the discovery of effective new inhibitors of this process.

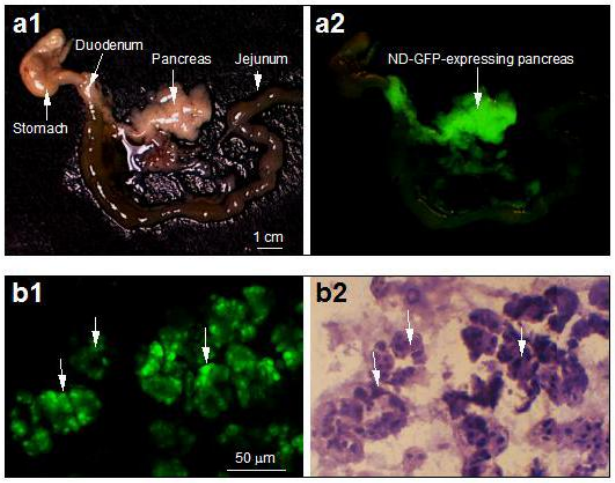

Figure 9. ND-GFP expression in the pancreas. The pancreas in ND-GFP transgenic nude mice, (a1) Bright field; (a2) fluorescence. Acinar cells of the pancreas in the ND-GFP transgenic nude mice (arrows), (b1) Fluorescence; (b2) Bright field.

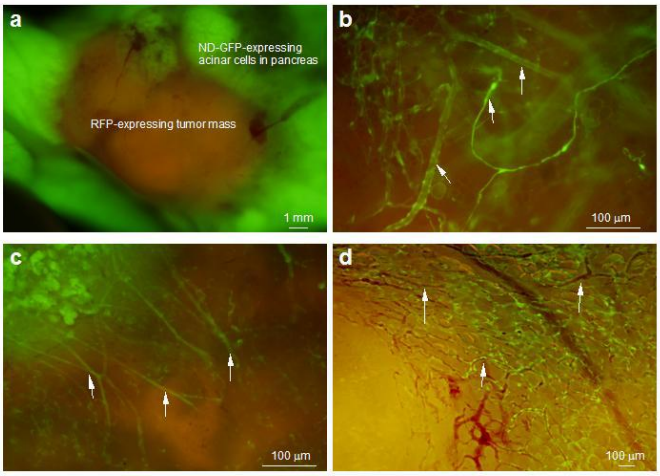

Figure 10. Dual-color imaging of nascent blood vessels in the orthotopically growing MIAPaCa-2 pancreatic tumor. (a-d) Day-14 after orthotopic implantation of RFP-expressing MIAPaCa-2 human pancreatic cancer cells to ND-GFP transgenic nude mice. (a) The RFP-expressing MIAPaCa-2 human pancreas tumor growing in the ND-GFP expressing pancreas in an ND-GFP transgenic nude mouse. (b-d) The ND-GFP-expressing nascent blood vessels (white arrows) growing in the RFP-expressing tumor mass. (d) Newly formed ND-GFP-expressing blood vessels with blood flow.

5. CONCLUSIONS

Here we describe our cumulative experience with the development and preclinical application of several highly fluorescent, clinically-relevant, orthotopic metastatic mouse models of pancreatic cancer. These models utilize the human pancreatic cancer cell lines which have been genetically engineered to selectively express high levels of the bioluminescent green fluorescent (GFP) or red fluorescent (RFP) proteins. Locoregional tumor growth and distant metastasis of these orthotopic implants occurs spontaneously and rapidly throughout the abdomen in a manner consistent with clinical human disease. Highly specific, high-resolution, real-time visualization of tumor growth and metastasis was achieved *in vivo* without the need for contrast agents, invasive techniques, or expensive imaging equipment. Transplantation of tumor fragments onto the pancreas of GFP-expressing transgenic mice may be used to facilitate visualization of tumor-host interaction between the pancreatic tumor fragments and host-derived stroma and vasculature. Such *in vivo* models have enabled us to serially visualize and acquire images of the progression of pancreatic cancer in the live animal, and to demonstrate the real-time antitumor, antimetastatic, and antiangiogenesis efficacy of several novel therapeutic strategies on pancreatic malignancy. These fluorescent models are therefore powerful and reliable tools with which to investigate human pancreatic cancer and therapeutic strategies directed against it.

REFERENCES

1. Bouvet, M., Gamagami, R. A., Gilpin, E. A., Romeo, O., Sasson, A., Easter, D. W., and Moossa, A. R. Factors influencing survival after resection for periampullary neoplasms. Am J Surg, *180:* 13-17, 2000.
2. Katz, M. H., Bouvet, M., Al-Refaie, W., Gilpin, E. A., and Moossa, A. R. Non-pancreatic periampullary adenocarcinomas: an explanation for favorable prognosis. Hepatogastroenterology, *51:* 842-846, 2004.

3. Bouvet, M., Binmoeller, K. F., and Moossa, A. R. Diagnosis of adenocarcinoma of the pancreas. *In:* J. L. Cameron (ed.), American Cancer Society Atlas of Clinical Oncology: Pancreatic Cancer. Hamilton, Ontario, Canada: BC Decker, 2001.
4. Moossa, A. R., Bouvet, M., and Gamagami, R. The pancreas. *In:* A. Cuschieri, R. J. C. Steele, and A. R. Moossa (eds.), Essential surgical practice, 4th edition, Vol. 2, pp. 477-525. London: Arnold Publishing, 2002.
5. Katz, M. H., Savides, T. J., Moossa, A. R., and Bouvet, M. An evidence-based approach to the diagnosis and staging of pancreatic cancer. Pancreatology, *5:* 576-590, 2005.
6. Bouvet, M., Yang, M., Nardin, S., Wang, X., Jiang, P., Baranov, E., Moossa, A. R., and Hoffman, R. M. Chronologically-specific metastatic targeting of human pancreatic tumors in orthotopic models. Clinical & Experimental Metastasis, *18:* 213-218, 2000.
7. Bouvet, M., Wang, J., Nardin, S. R., Nassirpour, R., Yang, M., Baranov, E., Jiang, P., Moossa, A. R., and Hoffman, R. M. Real-time optical imaging of primary tumor growth and multiple metastatic events in a pancreatic cancer orthotopic model. Cancer Res, *62:* 1534-1540, 2002.
8. Marincola, F. M., Drucker, B. J., Siao, D. Y., Hough, K. L., and Holder, W. D., Jr. The nude mouse as a model for the study of human pancreatic cancer. J Surg Res, *47:* 520-529, 1989.
9. Bruns, C. J., Harbison, M. T., Kuniyasu, H., Eue, I., and Fidler, I. J. In vivo selection and characterization of metastatic variants from human pancreatic adenocarcinoma by using orthotopic implantation in nude mice. Neoplasia, *1:* 50-62, 1999.
10. Vezeridis, M. P., Doremus, C. M., Tibbetts, L. M., Tzanakakis, G., and Jackson, B. T. Invasion and metastasis following orthotopic transplantation of human pancreatic cancer in the nude mouse. J Surg Oncol, *40:* 261-265, 1989.
11. Fu, X., Guadagni, F., and Hoffman, R. M. A metastatic nude-mouse model of human pancreatic cancer constructed orthotopically with histologically intact patient specimens. Proc Natl Acad Sci U S A, *89:* 5645-5649, 1992.
12. An, Z., Wang, X., Kubota, T., Moossa, A. R., and Hoffman, R. M. A clinical nude mouse metastatic model for highly malignant human pancreatic cancer. Anticancer Res, *16:* 627-631, 1996.
13. Furukawa, T., Kubota, T., Watanabe, M., Kitajima, M., and Hoffman, R. M. A novel patient-like treatment model of human pancreatic cancer constructed using orthotopic transplantation of histologically intact human tumor tissue in nude mice. Cancer Res, *53:* 3070-3072, 1993.
14. Kiguchi, K., Kubota, T., Aoki, D., Udagawa, Y., Yamanouchi, S., Saga, M., Amemiya, A., Sun, F. X., Nozawa, S., Moossa, A. R., and Hoffman, R. M. A patient-like orthotopic implantation nude mouse model of highly metastatic human ovarian cancer. Clin Exp Metastasis, *16:* 751-756, 1998.
15. Tomikawa, M., Kubota, T., Matsuzaki, S. W., Takahasi, S., Kitajima, M., Moosa, A. R., and Hoffman, R. M. Mitomycin C and cisplatin increase survival in a human pancreatic cancer metastatic model. Anticancer Res, *17:* 3623-3625, 1997.
16. Kyriazis, A. P., DiPersio, L., Michael, G. J., Pesce, A. J., and Stinnett, J. D. Growth patterns and metastatic behavior of human tumors growing in athymic mice. Cancer Res, *38:* 3186-3190., 1978.
17. Fidler, I. J. Critical factors in the biology of human cancer metastasis: twenty- eighth G.H.A. Clowes memorial award lecture. Cancer Res, *50:* 6130-6138., 1990.
18. Morikawa, K., Walker, S. M., Nakajima, M., Pathak, S., Jessup, J. M., and Fidler, I. J. Influence of organ environment on the growth, selection, and metastasis of human colon carcinoma cells in nude mice. Cancer Res, *48:* 6863-6871., 1988.
19. Tan, M. H. and Chu, T. M. Characterization of the tumorigenic and metastatic properties of a human pancreatic tumor cell line (AsPC-1) implanted orthotopically into nude mice. Tumour Biol, *6:* 89-98, 1985.
20. Lin, W. C., Pretlow, T. P., Pretlow, T. G., 2nd, and Culp, L. A. Bacterial lacZ gene as a highly sensitive marker to detect micrometastasis formation during tumor progression. Cancer Res, *50:* 2808-2817., 1990.
21. Fukumura, D., Yuan, F., Monsky, W. L., Chen, Y., and Jain, R. K. Effect of host microenvironment on the microcirculation of human colon adenocarcinoma. Am J Pathol, *151:* 679-688., 1997.
22. Chambers, A. F., MacDonald, I. C., Schmidt, E. E., Koop, S., Morris, V. L., Khokha, R., and Groom, A. C. Steps in tumor metastasis: new concepts from intravital videomicroscopy. Cancer Metastasis Rev, *14:* 279-301., 1995.
23. Weissleder, R., Tung, C. H., Mahmood, U., and Bogdanov, A., Jr. In vivo imaging of tumors with protease-activated near-infrared fluorescent probes. Nat Biotechnol, *17:* 375-378., 1999.

24. Sweeney, T. J., Mailander, V., Tucker, A. A., Olomu, A. B., Zhang, W., Cao, Y., Negrin, R. S., and Contag, C. H. Visualizing the kinetics of tumor-cell clearance in living animals. Proc Natl Acad Sci U S A, *96:* 12044-12049., 1999.
25. Cheng, L., Fu, J., Tsukamoto, A., and Hawley, R. G. Use of green fluorescent protein variants to monitor gene transfer and expression in mammalian cells. Nat Biotechnol, *14:* 606-609., 1996.
26. Chalfie, M., Tu, Y., Euskirchen, G., Ward, W. W., and Prasher, D. C. Green fluorescent protein as a marker for gene expression. Science, *263:* 802-805., 1994.
27. Astoul, P., Colt, H. G., Wang, X., and Hoffman, R. M. A "patient-like" nude mouse model of parietal pleural human lung adenocarcinoma. Anticancer Res, *14:* 85-91., 1994.
28. Yang, F., Moss, L. G., and Phillips, G. N., Jr. The molecular structure of green fluorescent protein. Nat Biotechnol, *14:* 1246-1251., 1996.
29. Prasher, D. C., Eckenrode, V. K., Ward, W. W., Prendergast, F. G., and Cormier, M. J. Primary structure of the Aequorea victoria green-fluorescent protein. Gene, *111:* 229-233., 1992.
30. Zolotukhin, S., Potter, M., Hauswirth, W. W., Guy, J., and Muzyczka, N. A "humanized" green fluorescent protein cDNA adapted for high-level expression in mammalian cells. J Virol, *70:* 4646-4654., 1996.
31. Heim, R., Cubitt, A. B., and Tsien, R. Y. Improved green fluorescence. Nature, *373:* 663-664., 1995.
32. Delagrave, S., Hawtin, R. E., Silva, C. M., Yang, M. M., and Youvan, D. C. Red-shifted excitation mutants of the green fluorescent protein. Biotechnology (N Y), *13:* 151-154., 1995.
33. Cormack, B. P., Valdivia, R. H., and Falkow, S. FACS-optimized mutants of the green fluorescent protein (GFP). Gene, *173(1:* 33-38., 1996.
34. Budinger, T. F., Benaron, D. A., and Koretsky, A. P. Imaging transgenic animals. Annual Review of Biomedical Engineering, *1:* 611-648, 1999.
35. Flotte, T. R., Beck, S. E., Chesnut, K., Potter, M., Poirier, A., and Zolotukhin, S. A fluorescence video-endoscopy technique for detection of gene transfer and expression. Gene Ther, *5:* 166-173, 1998.
36. Fu, X. Y., Besterman, J. M., Monosov, A., and Hoffman, R. M. Models of human metastatic colon cancer in nude mice orthotopically constructed by using histologically intact patient specimens. Proc Natl Acad Sci U S A, *88:* 9345-9349, 1991.
37. Sun, F. X., Sasson, A. R., Jiang, P., An, Z., Gamagami, R., Li, L., Moossa, A. R., and Hoffman, R. M. An ultra-metastatic model of human colon cancer in nude mice. Clin Exp Metastasis, *17:* 41-48, 1999.
38. Chishima, T., Miyagi, Y., Wang, X., Yamaoka, H., Shimada, H., Moossa, A. R., and Hoffman, R. M. Cancer invasion and micrometastasis visualized in live tissue by green fluorescent protein expression. Cancer Res, *57:* 2042-2047, 1997.
39. Chishima, T., Miyagi, Y., Wang, X., Baranov, E., Tan, Y., Shimada, H., Moossa, A. R., and Hoffman, R. M. Metastatic patterns of lung cancer visualized live and in process by green fluorescence protein expression. Clin Exp Metastasis, *15:* 547-552, 1997.
40. Chishima, T., Miyagi, Y., Wang, X., Tan, Y., Shimada, H., Moossa, A., and Hoffman, R. M. Visualization of the metastatic process by green fluorescent protein expression. Anticancer Res, *17:* 2377-2384, 1997.
41. Chishima, T., Miyagi, Y., Li, L., Tan, Y., Baranov, E., Yang, M., Shimada, H., Moossa, A. R., and Hoffman, R. M. Use of histoculture and green fluorescent protein to visualize tumor cell host interaction [letter]. In Vitro Cell Dev Biol Anim, *33:* 745-747, 1997.
42. Chishima, T., Yang, M., Miyagi, Y., Li, L., Tan, Y., Baranov, E., Shimada, H., Moossa, A. R., Penman, S., and Hoffman, R. M. Governing step of metastasis visualized in vitro. Proc Natl Acad Sci U S A, *94:* 11573-11576, 1997.
43. Yang, M., Hasegawa, S., Jiang, P., Wang, X., Tan, Y., Chishima, T., Shimada, H., Moossa, A. R., and Hoffman, R. M. Widespread skeletal metastatic potential of human lung cancer revealed by green fluorescent protein expression. Cancer Res, *58:* 4217-4221, 1998.
44. Yang, M., Jiang, P., Sun, F. X., Hasegawa, S., Baranov, E., Chishima, T., Shimada, H., Moossa, A. R., and Hoffman, R. M. A fluorescent orthotopic bone metastasis model of human prostate cancer. Cancer Res, *59:* 781-786, 1999.
45. Yang, M., Jiang, P., An, Z., Baranov, E., Li, L., Hasegawa, S., Al-Tuwaijri, M., Chishima, T., Shimada, H., Moossa, A. R., and Hoffman, R. M. Genetically fluorescent melanoma bone and organ metastasis models. Clin Cancer Res, *5:* 3549-3559, 1999.

46. Yang, M., Baranov, E., Jiang, P., Sun, F. X., Li, X. M., Li, L., Hasegawa, S., Bouvet, M., Al-Tuwaijri, M., Chishima, T., Shimada, H., Moossa, A. R., Penman, S., and Hoffman, R. M. Whole-body optical imaging of green fluorescent protein-expressing tumors and metastases. Proc Natl Acad Sci U S A, *97:* 1206-1211, 2000.
47. Yang, M., Baranov, E., Moossa, A. R., Penman, S., and Hoffman, R. M. Visualizing gene expression by whole-body fluorescence imaging [In Process Citation]. Proc Natl Acad Sci U S A, *97:* 12278-12282, 2000.
48. Yang, M., Baranov, E., Li, X. M., Wang, J. W., Jiang, P., Li, L., Moossa, A. R., Penman, S., and Hoffman, R. M. Whole-body and intravital optical imaging of angiogenesis in orthotopically implanted tumors. Proc Natl Acad Sci U S A, *98:* 2616-2621., 2001.
49. Yang, M., Baranov, E., Wang, J. W., Jiang, P., Wang, X., Sun, F. X., Bouvet, M., Moossa, A. R., Penman, S., and Hoffman, R. M. Direct external imaging of nascent cancer, tumor progression, angiogenesis, and metastasis on internal organs in the fluorescent orthotopic model. Proc Natl Acad Sci U S A, *99:* 3824-3829., 2002.
50. Katz, M. H., Takimoto, S., Spivack, D., Moossa, A. R., Hoffman, R. M., and Bouvet, M. A novel red fluorescent protein orthotopic pancreatic cancer model for the preclinical evaluation of chemotherapeutics. J Surg Res, *113:* 151-160, 2003.
51. Katz, M. H., Spivack, D. E., Takimoto, S., Fang, B., Burton, D. W., Moossa, A. R., Hoffman, R. M., and Bouvet, M. Gene therapy of pancreatic cancer with green fluorescent protein and tumor necrosis factor-related apoptosis-inducing ligand fusion gene expression driven by a human telomerase reverse transcriptase promoter. Ann Surg Oncol, *10:* 762-772, 2003.
52. Katz, M. H., Takimoto, S., Spivack, D., Moossa, A. R., Hoffman, R. M., and Bouvet, M. An imageable highly metastatic orthotopic red fluorescent protein model of pancreatic cancer. Clin Exp Metastasis, *21:* 7-12, 2004.
53. Tsuji, K., Yang, M., Jiang, P., Maitra, A., Kaushal, S., Yamauchi, K., Katz, M. H., Moossa, A. R., Hoffman, R. M., and Bouvet, M. Common bile duct injection as a novel method for establishing red fluorescent protein (RFP)-expressing human pancreatic cancer in nude mice. Jop, *7:* 193-199, 2006.
54. Bouvet, M., Spernyak, J., Katz, M. H., Mazurchuk, R. V., Takimoto, S., Bernacki, R., Rustum, Y. M., Moossa, A. R., and Hoffman, R. M. High correlation of whole-body red fluorescent protein imaging and magnetic resonance imaging on an orthotopic model of pancreatic cancer. Cancer Res, *65:* 9829-9833, 2005.
55. Katz, M. H., Bouvet, M., Takimoto, S., Spivack, D., Moossa, A. R., and Hoffman, R. M. Selective Antimetastatic Activity of Cytosine Analog CS-682 in a Red Fluorescent Protein Orthotopic Model of Pancreatic Cancer. Cancer Res, *63:* 5521-5525, 2003.
56. Katz, M. H., Bouvet, M., Takimoto, S., Spivack, D., Moossa, A. R., and Hoffman, R. M. Survival efficacy of adjuvant cytosine-analogue CS-682 in a fluorescent orthotopic model of human pancreatic cancer. Cancer Res, *64:* 1828-1833, 2004.
57. Amoh, Y., Li, L., Tsuji, K., Moossa, A. R., Katsuoka, K., Hoffman, R. M., and Bouvet, M. Dual-color imaging of nascent blood vessels vascularizing pancreatic cancer in an orthotopic model demonstrates antiangiogenesis efficacy of gemcitabine. J Surg Res, *132:* 164-169, 2006.
58. Amoh, Y., Nagakura, C., Maitra, A., Moossa, A. R., Katsuoka, K., Hoffman, R. M., and Bouvet, M. Dual-color imaging of nascent angiogenesis and its inhibition in liver metastases of pancreatic cancer. Anticancer Res, *26:* 3237-3242, 2006.
59. Yang, M., Li, L., Jiang, P., Moossa, A. R., Penman, S., and Hoffman, R. M. Dual-color fluorescence imaging distinguishes tumor cells from induced host angiogenic vessels and stromal cells. Proc Natl Acad Sci U S A, 2003.
60. Saito, N., Zhao, M., Li, L., Baranov, E., Yang, M., Ohta, Y., Katsuoka, K., Penman, S., and Hoffman, R. M. High efficiency genetic modification of hair follicles and growing hair shafts. Proc Natl Acad Sci U S A, *99:* 13120-13124, 2002.
61. Lee, N. C., Bouvet, M., Nardin, S., Jiang, P., Baranov, E., Rashidi, B., Yang, M., Wang, X., Moossa, A. R., and Hoffman, R. M. Antimetastatic efficacy of adjuvant gemcitabine in a pancreatic cancer orthotopic model. Clin Exp Metastasis, *18:* 379-384, 2000.